Efficiency of Spin-Transfer-Torque Switching and Thermal-Stability Factor in a Spin-Valve Nanopillar with First- and Second-Order Uniaxial Magnetic Anisotropies

Rie Matsumoto,[1] Hiroko Arai,[2,1] Shinji Yuasa,[1] and Hiroshi Imamura[1,*]

[1]*National Institute of Advanced Industrial Science and Technology (AIST), Spintronics Research Center, Tsukuba, Ibaraki 305-8568, Japan*
[2]*PRESTO, JST, Honcho, Kawaguchi, Saitama 332-0012, Japan*

The efficiency of spin-transfer-torque (STT) switching and the thermal-stability factor are important figures of merit in STT-based magnetoresistive random-access memory. We derive analytical expressions of the STT-switching efficiency and the thermal-stability factor for a perpendicularly magnetized spin-valve nanopillar with the first- and the second-order uniaxial magnetic anisotropy. It is shown that the STT-switching efficiency is maximized when the effective first-order anisotropy constant ($K_{u1,\text{eff}}$) is equal to the second-order anisotropy constant (K_{u2}). It is also shown that the thermal-stability factor is most (least) sensitive to a variation of the applied current when $K_{u2} = -0.41$ (0.70) $K_{u1,\text{eff}}$.

I. INTRODUCTION

Spin-transfer-torque (STT) switching has been attracting a great deal of attention due to its potential application to STT-based magnetoresistive random-access memory (STT MRAM) [1–11]. The basic structure of memory cells in STT MRAM is a spin-valve nanopillar (SVNP), where a nonmagnetic spacer layer is sandwiched between two ferromagnetic layers, called a free layer (FL) and a reference layer (RL), as shown in Fig. 1(a). Usually, the magnetization of the FL is perpendicularly or conically magnetized, and the magnetization of the RL is perpendicularly magnetized.

In STT MRAM, the magnetization of the FL is switched by STT once the applied current (I) exceeds the threshold level, called the switching current (I_{sw}) [13,14]. The data retention time of the FL in a SVNP is characterized by the thermal-stability factor in the absence of current, Δ_0, which is defined by the energy barrier height normalized by the thermal energy at room temperature. The STT-switching efficiency given by $\kappa = \Delta_0/I_{\text{sw}}$ is an important figure of merit in STT MRAM [15], and a considerable amount of effort has been devoted to enhance κ.

Even when I is lower than I_{sw}, thermal agitation induces magnetization switching with a certain probability. Such thermally activated switching is the origin of read disturbance; i.e., the accidental switching of the magnetization during the readout operation. The read disturbance is one of the most serious issues for high-density STT MRAM because the difference between the read and write currents should be decreased for a smaller lateral size of a SVNP [16,17]. Starting from the Fokker-Planck equation, the probability of thermally activated switching (P_{sw}) is derived as $P_{\text{sw}} = 1 - \exp\left[-f\tau\exp(-\Delta)\right]$, where f is the attempt frequency, τ is the current pulse width, and Δ is the thermal-stability factor [18]. Since P_{sw} depends strongly on Δ, it is important to study the current dependence of Δ to control P_{sw}.

Most studies of STT switching in perpendicularly magnetized STT MRAM are based on the assumption that the magnetic anisotropy of the FL is expressed by the effective first-order anisotropy constant ($K_{u1,\text{eff}}$) by neglecting the higher-order magnetic anisotropies. However, recent experimental studies observed the large second-order uniaxial magnetic anisotropy constant (K_{u2}) in a Co-Fe-B thin film, which is commonly used as a FL in STT MRAMs [19–21]. A subsequent theoretical study pointed out that K_{u2} can enhance κ for the case of $|K_{u2}/K_{u1,\text{eff}}| \ll 1$ [22]. The experimental results also showed that the FL can be conically magnetized within a certain range of film thickness [19–21]. The switching properties of the STT MRAM with conically magnetized FL (CFL) [23] was theoretically studied by the present authors [14,24]. However, κ and Δ of the perpendicularly magnetized FL (PFL) with K_{u2} are not fully understood. In this paper, the analytical expressions of κ and Δ for PFL with K_{u2} are derived. It is shown that κ is a function of $r_K = K_{u2}/K_{u1,\text{eff}}$. κ is larger than that for PFL without K_{u2} for a positive r_K and takes a maximum value at $r_K = 1$. It is also shown that Δ is well approximated as $\Delta_0(1 - I/I_{\text{sw}})^\eta$, and η is also a function of r_K. The value of η for the whole range of r_K is obtained.

II. MODEL

The system we consider is schematically illustrated in Fig. 1(a). The lateral size of a SVNP is assumed to be so small that the magnetization switching can be described
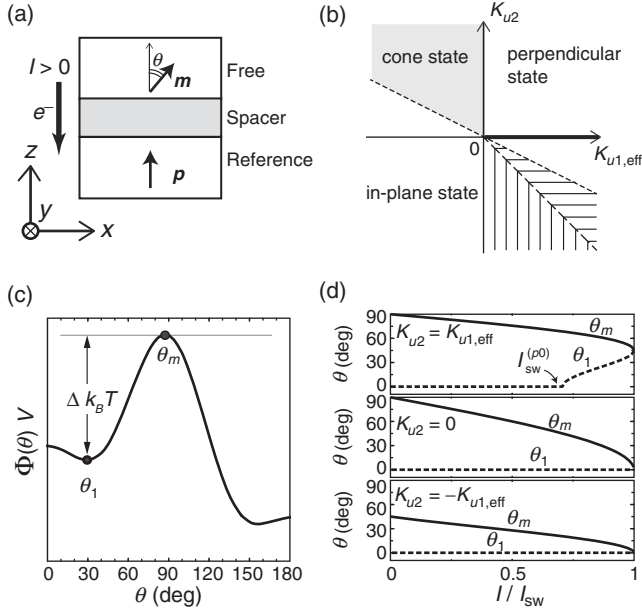
FIG. 1. (a) Schematic cross section of a spin-valve nanopillar and definitions of current polarity and Cartesian coordinates (x, y, z). (b) Phase diagram of magnetic film with the uniaxial anisotropy constants $K_{u1,\text{eff}}$ and K_{u2} (redrawn from Ref. [12]). The cone-state region is represented by shade, and the perpendicular state with $K_{u2} = 0$ is indicated by the thick solid line. Metastable regions are hatched. (c) Schematic illustration of θ dependence of $\Phi(\theta)V$ of the CFL. It has a minimum at $\theta = \theta_1$ in $0° \leq \theta < 90°$, and a maximum at $\theta = \theta_m$ in $\theta_1 \leq \theta \leq 90°$. Δ is defined by the energy barrier height normalized by the thermal energy, $k_B T$. (d) I/I_{sw} dependence of θ_m (the solid lines) and θ_1 (the dotted lines). For all panels, $K_{u1,\text{eff}} = 1.00$ Merg/cm³. From top to bottom, $K_{u2} = K_{u1,\text{eff}}$, 0, and $-K_{u1,\text{eff}}$, respectively.

by the macrospin model. The single-domain-type magnetization switching takes place up to $D \sim \delta_w$, where D is the diameter of a FL and δ_w is the domain-wall width [25]. For example, in a Co-Fe-B-based FL, $\delta_w \sim 30$ nm. Directions of the magnetization in the FL and the RL are represented by the unit vectors $\boldsymbol{m}$ and $\boldsymbol{p}$, respectively. The vector $\boldsymbol{p}$ is fixed to the positive z direction. The positive current, $I > 0$, is defined as electrons flowing from the FL to the RL. We assume $I > 0$ and analyze the switching of $\boldsymbol{m}$ from $m_z > 0$.

Since the system has uniaxial symmetry around the z axis, the equations of motion of $\boldsymbol{m}$ are given by the following Landau-Lifshitz-Gilbert (LLG) equation [26]:

$$\frac{d\theta}{dt} = -\alpha \frac{\gamma}{M_s} \frac{\partial \Phi}{\partial \theta}, \tag{1}$$

$$\sin\theta \frac{d\phi}{dt} = \frac{\gamma}{M_s} \frac{\partial g_L}{\partial \theta}. \tag{2}$$

Here, θ and ϕ are the polar and azimuthal angles of $\boldsymbol{m}$. The second-order terms pertaining to α and a_I are neglected. t is the time and γ is the gyromagnetic ratio.

α and M_s are the Gilbert damping constant and the saturation magnetization in the FL. The magnetic energy, g_L, and the effective potential, Φ, are defined as

$$g_L = K_{u1,\text{eff}} \sin^2\theta + K_{u2} \sin^4\theta, \tag{3}$$

$$\Phi = g_L + M_s \frac{a_I}{\alpha} \frac{\ln(1 + P^2 \cos\theta)}{P^2}, \tag{4}$$

where $K_{u1,\text{eff}}$ is defined as $K_{u1,\text{eff}} = K_{u1} - 2\pi M_s^2$, where K_{u1} is the first-order anisotropy constant. a_I is the coefficient of the STT, with $a_I = \hbar IP/(2|e|M_s V)$, where P is the spin polarization, e is the electron charge, V is the volume of the FL, and $\hbar$ is the Dirac constant.

Equation (1) shows that the polar angle θ yields a dynamics in the effective potential Φ and can be obtained separately from the azimuthal angle ϕ. The fixed points are expressed by the minima of Φ, and the switching current is determined by the condition for disappearance of the minimum point. Therefore, we analyze the effective potential Φ instead of the LLG equation. In order to obtain the analytical expression, the STT term in Φ is approximated as

$$M_s \frac{a_I}{\alpha} \frac{\ln(1 + P^2 \cos\theta)}{P^2} \simeq M_s \frac{a_I}{\alpha} \cos\theta, \tag{5}$$

where the spin polarization P is assumed to satisfy $P^2/2 \ll 1$ because the typical value of P is about 0.5. Thus, the effective potential is expressed as

$$\Phi = K_{u1,\text{eff}} \sin^2\theta + K_{u2} \sin^4\theta + M_s \frac{a_I}{\alpha} \cos\theta. \tag{6}$$

In Eq. (6), the fieldlike torque is neglected because its effect on the switching current and the switching probability is much smaller than that of the STT. The detailed discussion on the effect of the fieldlike torque will be given in the Appendix.

III. RESULTS AND DISCUSSIONS

A. Phase diagram

The equilibrium direction of $\boldsymbol{m}$ is determined by minimizing $g_L(\theta)$. The phase diagram of the equilibrium direction is shown in Fig. 1(b). The cone state is stable in the region satisfying $K_{u1,\text{eff}} < 0$ and $2K_{u2} > -K_{u1,\text{eff}}$, shown as a shaded area. The in-plane state is stabilized if $K_{u1,\text{eff}} < 0$ and $2K_{u2} \leq -K_{u1,\text{eff}}$. The perpendicular state is stable (metastable) in the region where $K_{u1,\text{eff}} \geq 0$ and $K_{u2} \geq -K_{u1,\text{eff}}$, excluding $K_{u1,\text{eff}} = K_{u2} = 0$ ($K_{u1,\text{eff}} > 0$ and $K_{u2} < -K_{u1,\text{eff}}$). Since the switching properties of the PFL with $K_{u2} = 0$ (the thick solid line) and the CFL (the shaded region) are already known, the present analysis concentrates on the PFL with K_{u2}.

B. Conically magnetized free layer

Before showing the detailed analysis, let us briefly review the κ and the Δ of the CFL [24] and the PFL with $K_{u2} = 0$ [13,15,27]. The θ dependence of the effective potential, $\Phi(\theta)V$, of the CFL is schematically shown in Fig. 1(c). Δ is defined as the energy barrier height, $[\Phi(\theta_m) - \Phi(\theta_1)]V$, normalized by the thermal energy, $k_B T$. k_B is the Boltzmann constant and T is the temperature. θ_1 is the polar angle where Φ is minimized in the range $0° \leq \theta < 90°$, and θ_m is the polar angle where Φ is maximized in the range $\theta_1 \leq \theta \leq 90°$. The thermal-stability factor at $I = 0$ is given by

$$\Delta_0^{(c)} = \frac{(K_{u1,\mathrm{eff}} + K_{u2} + \frac{K_{u1,\mathrm{eff}}^2}{4K_{u2}})V}{k_B T}. \tag{7}$$

The switching current is obtained by requiring that $\theta_1 = \theta_m$, as

$$I_{\mathrm{sw}}^{(c)} = \frac{8}{3\sqrt{6}} \frac{\alpha V |e|}{\hbar P} \sqrt{\frac{(K_{u1,\mathrm{eff}} + 2K_{u2})^3}{K_{u2}}}, \tag{8}$$

which is the same as that obtained from the LLG equation in Ref. [14].

From Eqs. (7) and (8), the switching efficiency is obtained as

$$\kappa^{(c)} = \frac{3\sqrt{6}}{32} \frac{\hbar P}{\alpha |e|} \frac{1}{k_B T} \sqrt{2 + \frac{K_{u1,\mathrm{eff}}}{K_{u2}}}, \tag{9}$$

which is a monotonic increasing function of K_{u2} since $K_{u1,\mathrm{eff}} < 0$ for the CFL. The thermal-stability factor at finite I is given by

$$\Delta^{(c)} = \frac{i\Delta_0^{(c)}}{\sqrt{3}} [A_-^{2/3} - A_+^{2/3} - 2\xi^{(c)}(A_-^{1/3} - A_+^{1/3})], \tag{10}$$

where $A_\pm = \xi^{(c)} \pm \sqrt{[\xi^{(c)}]^2 - 1}$, $\xi^{(c)} = I/I_{\mathrm{sw}}^{(c)}$. In Ref. [24], it is shown that Eq. (10) is well approximated as $\Delta_0^{(c)}(1 - I/I_{\mathrm{sw}}^{(c)})^\eta$. The exponent η is obtained as

$$\eta = -\lim_{\xi \to 0} \left(\frac{d}{d\xi} \frac{\Delta^{(c)}}{\Delta_0^{(c)}} \right) = \frac{8\sqrt{3}}{9} \simeq 1.53, \tag{11}$$

which is also obtained from the numerical fit of Eq. (10).

C. Perpendicularly magnetized free layer without second-order uniaxial magnetic anisotropy

For the PFL, the thermal-stability factor at $I = 0$ is given by

$$\Delta_0^{(p0)} = \frac{K_{u1,\mathrm{eff}} V}{k_B T}, \tag{12}$$

and the switching current [13] is

$$I_{\mathrm{sw}}^{(p0)} = \frac{4\alpha V |e|}{\hbar P} K_{u1,\mathrm{eff}}. \tag{13}$$

From Eqs. (12) and (13), the switching efficiency is obtained as

$$\kappa^{(p0)} = \frac{1}{4} \frac{\hbar P}{\alpha |e|} \frac{1}{k_B T}, \tag{14}$$

which is independent of $K_{u1,\mathrm{eff}}$. Comparing Eq. (9) to Eq. (14), one can see that $\kappa^{(c)} \geq \kappa^{(p0)}$ if $K_{u2}/K_{u1,\mathrm{eff}} \geq -27/22(\simeq -1.23)$. The thermal-stability factor at finite I is given by [27]

$$\Delta^{(p0)} = \Delta_0^{(p0)}(1 - I/I_{\mathrm{sw}}^{(p0)})^2. \tag{15}$$

It should be noted that the exponent of the current dependence of Δ/Δ_0 for the PFL with $K_{u2} = 0$ ($\eta = 2$) and CFL ($\eta = 1.53$) is independent of the values of $K_{u1,\mathrm{eff}}$ and K_{u2}. It is interesting to analyze how these different values of the exponent—i.e., 1.53 and 2—are related to each other.

D. Perpendicularly magnetized free layer with second-order uniaxial magnetic anisotropy

Let us analyze the switching efficiency and the thermal-stability factor of a PFL with a finite K_{u2}. Since we do not analyze either the cone state or the in-plane magnetized state, the effective first-order anisotropy constant is assumed to be positive; i.e., $K_{u1,\mathrm{eff}} \geq 0$ and $K_{u2} > 0$ or $K_{u1,\mathrm{eff}} > 0$ and $K_{u2} < 0$. Since the calculation procedure is similar to that presented in Ref. [24], we simply list the results without derivation.

The polar angle of the equilibrium direction is obtained as

$$\theta_1 = \begin{cases} \cos^{-1}\left(\frac{X^{1/3}}{3} - pX^{-1/3}\right) & \text{for } r_K > \frac{1}{4} \text{ and } I \geq I_{\mathrm{sw}}^{(p0)} \\ 0 & \text{otherwise} \end{cases}, \tag{16}$$

where $X = (3/2)(-9q + \sqrt{12p^3 + 81q^2})$, $p = -(K_{u1,\mathrm{eff}} + 2K_{u2})/(2K_{u2})$, and $q = a_I M_s/(4\alpha K_{u2})$. For $r_K > 1/4$, θ_1 increases with an increase of I once I exceeds $I_{\mathrm{sw}}^{(p0)}$, as shown in the top panel of Fig. 1(d). Otherwise, θ_1 is zero, as shown in the middle and bottom panels of Fig. 1(d).

The polar angle where Φ is maximized in the range $\theta_1 \leq \theta \leq 90°$ is given by

$$\theta_m = \begin{cases} \cos^{-1}\left(\frac{\omega^2 X^{1/3}}{3} - \omega p X^{-1/3}\right) & \text{for } r_K > 0 \\ \cos^{-1}\left(\frac{X^{1/3}}{3} - p X^{-1/3}\right) & \text{for } r_K < 0 \end{cases}, \quad (17)$$

where $\omega = (-1 + i\sqrt{3})/2$. θ_m is a monotonically decreasing function of I, as shown in Fig. 1(d). Especially at $I = 0$, θ_m is expressed as

$$\theta_m = \begin{cases} \frac{\pi}{2} & \text{for } r_K \geq -1/2 \\ \sin^{-1}\sqrt{-\frac{1}{2}\frac{K_{u1,\text{eff}}}{K_{u2}}} & \text{for } r_K < -1/2 \end{cases}, \quad (18)$$

where $r_K = -1/2$ is the boundary of the metastable state shown in Fig. 1(b). The thermal-stability factor at $I = 0$ is given by $[g_L(\theta_m) - g_L(0)]/(k_B T)$ as

$$\Delta_0 = \begin{cases} \frac{(K_{u1,\text{eff}} + K_{u2})V}{k_B T} & \text{for } r_K \geq -1/2 \\ -\frac{K_{u1,\text{eff}}^2 V}{4K_{u2}k_B T} & \text{for } r_K < -1/2 \end{cases}. \quad (19)$$

The switching current is obtained by requiring $\Phi(\theta_m) - \Phi(\theta_1) = 0$, as

$$I_{\text{sw}} = \begin{cases} I_{\text{sw}}^{(c)} & \text{for } r_K > 1/4 \\ I_{\text{sw}}^{(p0)} & \text{for } r_K \leq 1/4 \end{cases}, \quad (20)$$

where $I_{\text{sw}}^{(c)}$ and $I_{\text{sw}}^{(p0)}$ are defined in Eqs. (8) and (13), respectively.

The boundary of $r_K = 1/4$ in Eq. (20) can be intuitively understood from the viewpoint of the competition between the STT and the damping torque. Equation (1) is expressed as

$$\frac{d\theta}{dt} = \gamma \sin\theta(a_I + \alpha H_\theta/\sin\theta), \quad (21)$$

where $H_\theta = -(1/M_s)(\partial g_L/\partial\theta)$ and $H_\theta/\sin\theta = -2\cos\theta$ $(K_{u1,\text{eff}} + 2K_{u2}\sin^2\theta)/M_s$. Once a_I exceeds the coefficient of the damping torque—that is, $\alpha H_\theta/\sin\theta$—the magnetization switches. The function $H_\theta/\sin\theta$ takes its minimum value at

$$\theta = \begin{cases} \sin^{-1}\sqrt{\frac{-K_{u1,\text{eff}} + 4K_{u2}}{6K_{u2}}} & \text{for } r_K > 1/4 \\ 0 & \text{for } r_K \leq 1/4 \end{cases}. \quad (22)$$

This boundary of $r_K = 1/4$ in Eq. (22) is the origin of the boundary in Eq. (20). It should be noted that, for $r_K > 1/4$, the oscillating state with a finite cone angle of θ_1 is stabilized by the STT if $I_{\text{sw}}^{(p0)} < I < I_{\text{sw}}^{(c)}$.

From Eqs. (19) and (20), the switching efficiency normalized by $\kappa^{(p0)}$ is obtained as
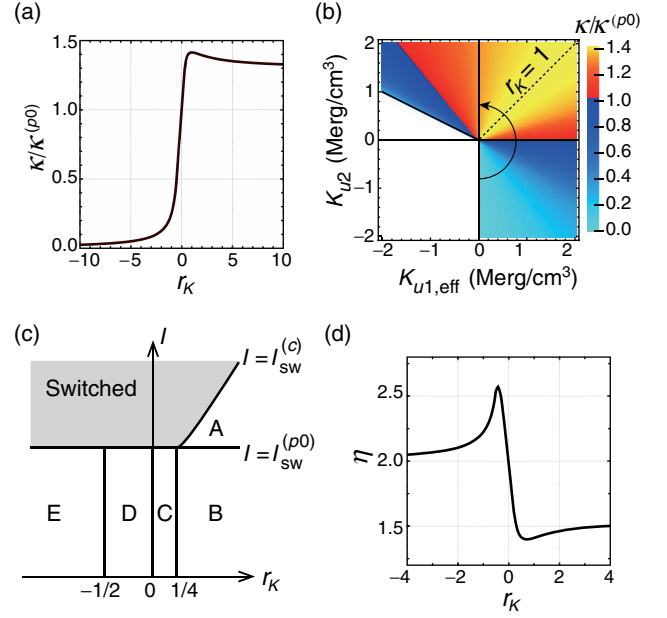

FIG. 2. (a) r_K dependence of the normalized switching efficiency, $\kappa/\kappa^{(p0)}$. (b) Color map of the normalized switching efficiency, $\kappa/\kappa^{(p0)}$, on the $K_{u1,\text{eff}} - K_{u2}$ plane. The value of $\kappa/\kappa^{(p0)}$ that is less (more) than unity is represented by the blue (red) tones. The semicircle with an arrow head represents the trajectory corresponding to $r_K = -\infty \to \infty$. The dotted line represents the condition for maximizing $\kappa/\kappa^{(p0)}$, i.e., $r_K = 1$. (c) Classification of the $I - r_K$ space for the calculation of Δ. In the shaded region, the magnetization is switched. In the regions A, B, C, D, and E, Δ takes different analytical expressions. (d) The r_K dependence of exponent η of the current dependence of Δ/Δ_0 obtained by a numerical fit.

$$\frac{\kappa}{\kappa^{(p0)}} = \begin{cases} \frac{3\sqrt{6}}{2}\frac{\sqrt{r_K}(1+r_K)}{(1+2r_K)^{3/2}} & \text{for } r_K > 1/4 \\ 1 + r_K & \text{for } -1/2 \leq r_K \leq 1/4 \\ -\frac{1}{4r_K} & \text{for } r_K < -1/2 \end{cases}. \quad (23)$$

In Fig. 2(a), the normalized switching efficiency, $\kappa/\kappa^{(p0)}$, of the PFL given in Eq. (23) is plotted as a function of r_K. It should be noted that $\kappa/\kappa^{(p0)}$ is larger than unity for a positive r_K and takes a maximum value of $\sqrt{2}$ at $r_K = 1$. The limiting values are as follows: $\lim_{r_K \to -\infty}\kappa/\kappa^{(p0)} = 0$, and $\lim_{r_K \to \infty}\kappa/\kappa^{(p0)} = 3\sqrt{3}/4 \simeq 1.30$.

Figure 2(b) shows a color map of $\kappa/\kappa^{(p0)}$ on the $K_{u1,\text{eff}} - K_{u2}$ plane. The results of the CFL are also plotted in Fig. 2(b) for convenience. The value of $\kappa/\kappa^{(p0)}$ that is less (more) than unity is represented by the blue (red) tones. Starting from a certain point with $K_{u1,\text{eff}} = 0$ and $K_{u2} < 0$, which corresponds to $r_K = -\infty$, and moving along the semicircle, the normalized switching efficiency increases from 0 with an increase of r_K and takes a maximum value of $\sqrt{2}$ at $r_K = 1$. Then it deceases with an increase of r_K to the limiting value of $3\sqrt{3}/4 \simeq 1.30$, as shown in Fig. 2(a).

In order to calculate the thermal-stability factor, the $I - r_K$ plane is divided into six regions, as shown in Fig. 2(c). The switched region is shaded. The normalized thermal-stability factor, Δ/Δ_0, in the regions A, B, C, D, and E is obtained as follows. In region A, $r_K > 1/4$ and $I \geq I_{\mathrm{sw}}^{(p0)}$,

$$\frac{\Delta}{\Delta_0} = \frac{(1 + 2r_K)^2}{r_K(1 + r_K)} \left\{ \frac{1}{\sqrt{6}} \xi \left[\frac{\omega - 1}{2\Lambda} + \frac{(\omega^2 - 1)\Lambda}{3} \right] \right. $$
$$\left. - \frac{1}{2} \left[\frac{\omega^2 - 1}{4\Lambda^2} + \frac{(\omega - 1)\Lambda^2}{9} \right] \right\}, \tag{24}$$

where $\xi = I/I_{\mathrm{sw}}$ and

$$\Lambda = \sqrt{\frac{3}{2}} \left(\sqrt{\xi^2 - 1} - \xi \right)^{1/3}. \tag{25}$$

In region B, $r_K > 1/4$ and $I < I_{\mathrm{sw}}^{(p0)}$,

$$\frac{\Delta}{\Delta_0} = 1 - \frac{1 + 2r_K}{1 + r_K} \left\{ \frac{4\xi}{3} \sqrt{\frac{1 + 2r_K}{6r_K}} - \frac{1 + 2r_K}{r_K} \right.$$
$$\left. \times \left(\frac{\omega}{2\Lambda} + \frac{\omega^2\Lambda}{3} \right) \left[\frac{\xi}{\sqrt{6}} - \frac{\omega}{4\Lambda} - \frac{\omega^2\Lambda}{6} \right] \right\}. \tag{26}$$

In region C, $0 < r_K \leq 1/4$,

$$\frac{\Delta}{\Delta_0} = 1 - \frac{1}{1 + r_K} \left[2\xi - \frac{3\xi}{2} \left(\frac{\omega^2 X^{1/3}}{3} - \omega p X^{-1/3} \right) \right.$$
$$\left. + \frac{1}{2}(1 + 2r_K) \left(\frac{\omega^2 X^{1/3}}{3} - \omega p X^{-1/3} \right)^2 \right]. \tag{27}$$

In region D, $-1/2 \leq r_K < 0$,

$$\frac{\Delta}{\Delta_0} = 1 - \frac{1}{1 + r_K} \left[2\xi - \frac{3\xi}{2} \left(\frac{X^{1/3}}{3} - p X^{-1/3} \right) \right.$$
$$\left. + \frac{(1 + 2r_K)}{2} \left(\frac{X^{1/3}}{3} - p X^{-1/3} \right)^2 \right]. \tag{28}$$

In region E, $r_K < -1/2$,

$$\frac{\Delta}{\Delta_0} = -4r_K \left[1 + r_K - 2\xi + \frac{3\xi}{2} \left(\frac{X^{1/3}}{3} - p X^{-1/3} \right) \right.$$
$$\left. - \frac{(1 + 2r_K)}{2} \left(\frac{X^{1/3}}{3} - p X^{-1/3} \right)^2 \right]. \tag{29}$$

The curves representing Δ/Δ_0 are well fitted to the function of $(1 - I/I_{\mathrm{sw}})^\eta$. The obtained exponent η is plotted in Fig. 2(d) as a function of r_K. η takes the minimum value of 1.40 at $r_K = 0.70$ and the maximum value of 2.57 at $r_K = -0.41$. As a result, the thermal-stability factor, Δ, and therefore the switching probability, P_{sw}, are most (least)

sensitive to the variation of applied current at $r_K = -0.41$ (0.70). From Eqs. (24) and (29), the limiting values of η are obtained as $\lim_{r_K \to \infty} \eta = 1.53$ and $\lim_{r_K \to -\infty} \eta = 2$.

IV. CONCLUSION

In summary, the analytical expression of the STT-switching efficiency and the thermal-stability factor are derived for a perpendicularly magnetized SVNP with a second-order uniaxial magnetic anisotropy. The switching efficiency is maximized at $K_{u1,\mathrm{eff}} = K_{u2}$. The maximum value is $\sqrt{2}$ times larger than that without K_{u2}. Fitting the obtained thermal-stability factor to the function of $\Delta_0(1 - I/I_{\mathrm{sw}})^\eta$, the exponent η is calculated for the whole range of r_K's. The exponent η takes its minimum value of 1.40 at $r_K = 0.70$ and its maximum value of 2.57 at $r_K = -0.41$; i.e., the switching probability is most (least) sensitive to a variation of the applied current at $r_K = -0.41$ (0.70).

APPENDIX: EFFECT OF FIELDLIKE TORQUE

In this appendix, the effect of fieldlike torque (FLT) on the switching current is considered. In the presence of FLT, the LLG equation is given by the same Eqs. (1) and (2) except that g_L is given by [26]

$$g_L = K_{u1,\mathrm{eff}} \sin^2 \theta + K_{u2} \sin^4 \theta - M_s b_I \cos \theta, \tag{A1}$$

where b_I is the coefficient of the FLT, which is conventionally expressed as $b_I = \beta a_I$. β is typically approximately 0.1 in current-perpendicular-to-plane giant-magnetoresistance SVNPs [28,29], and, typically, 0.2–0.3 in MgO-based magnetic tunnel junctions [30,31]. The LLG equation including FLT is expressed as

$$\frac{d\theta}{dt} = \gamma(a_I - \alpha b_I) \sin \theta + \gamma \alpha H_\theta, \tag{A2}$$

$$\sin \theta \frac{d\phi}{dt} = -\gamma H_\theta + \gamma b_I \sin \theta, \tag{A3}$$

where $H_\theta/\sin \theta = -2 \cos \theta (K_{u1,\mathrm{eff}} + 2K_{u2} \sin^2 \theta)/M_s$. In Eq. (A2), which determines the switching current and the switching probability, the magnitude of the FLT is much smaller than that of the STT because $\alpha b_I \ll a_I$. From Eq. (A2), the switching current is obtained as

$$I_{\mathrm{sw}} = \begin{cases} \frac{1}{1 - \alpha\beta} I_{\mathrm{sw}}^{(c)} & \text{for } r_K > 1/4 \\ \frac{1}{1 - \alpha\beta} I_{\mathrm{sw}}^{(p0)} & \text{for } r_K \leq 1/4 \end{cases}. \tag{A4}$$

The effect of FLT on the switching current is negligible because $\alpha\beta$ is much smaller than unity.

[1] J. C. Slonczewski, Current-driven excitation of magnetic multilayers, J. Magn. Magn. Mater. **159**, L1 (1996).

[2] L. Berger, Emission of spin waves by a magnetic multilayer traversed by a current, Phys. Rev. B **54**, 9353 (1996).

[3] E. B. Myers, D. C. Ralph, J. A. Katine, R. N. Louie, and R. A. Buhrman, Current-induced switching of domains in magnetic multilayer devices, Science **285**, 867 (1999).

[4] Yiming Huai, Frank Albert, Paul Nguyen, Mahendra Pakala, and Thierry Valet, Observation of spin-transfer switching in deep submicron-sized and low-resistance magnetic tunnel junctions, Appl. Phys. Lett. **84**, 3118 (2004).

[5] Hitoshi Kubota, Akio Fukushima, Yuichi Ootani, Shinji Yuasa, Koji Ando, Hiroki Maehara, Koji Tsunekawa, David D. Djayaprawira, Naoki Watanabe, and Yoshishige Suzuki, Evaluation of spin-transfer switching in CoFeB/ MgO/CoFeB magnetic tunnel junctions, Jpn. J. Appl. Phys. **44**, L1237 (2005).

[6] Jun Hayakawa, Shoji Ikeda, Young Min Lee, Ryutaro Sasaki, Toshiyasu Meguro, Fumihiro Matsukura, Hiromasa Takahashi, and Hideo Ohno, Current-driven magnetization switching in CoFeB/MgO/CoFeB magnetic tunnel junctions, Jpn. J. Appl. Phys. **44**, L1267 (2005).

[7] M. Hosomi, H. Yamagishi, T. Yamamoto, K. Bessho, Y. Higo, K. Yamane, H. Yamada, M. Shoji, H. Hachino, C. Fukumoto, H. Nagao, and H. Kano, in *Proceedings of the IEEE International Electron Devices Meeting, Washington, DC, 2005* (IEEE, New York, 2005), p. 459.

[8] T. Kishi *et al.*, in *Proceedings of the IEEE International Electron Devices Meeting, San Francisco, 2008* (IEEE, New York, 2008).

[9] S. Ikeda, K. Miura, H. Yamamoto, K. Mizunuma, H. D. Gan, M. Endo, S. Kanai, J. Hayakawa, F. Matsukura, and H. Ohno, A perpendicular-anisotropy CoFeB-MgO magnetic tunnel junction, Nat. Mater. **9**, 721 (2010).

[10] E. Kitagawa, S. Fujita, K. Nomura, H. Noguchi, K. Abe, K. Ikegami, T. Daibou, Y. Kato, C. Kamata, S. Kashiwada, N. Shimomura, J. Ito, and H. Yoda, in *Proceedings of the International Electron Devices Meeting, San Francisco, 2012* (IEEE, New York, 2012), p. 29.4.1.

[11] Kay Yakushiji, Akio Fukushima, Hitoshi Kubota, Makoto Konoto, and Shinji Yuasa, Ultralow-voltage spin-transfer switching in perpendicularly magnetized magnetic tunnel junctions with synthetic antiferromagnetic reference layer, Appl. Phys. Express **6**, 113006 (2013).

[12] H. B. G. Casimir, J. Smit, U. Enz, J. F. Fast, H. P. J. Wijn, E. W. Gorter, A. J. W. Duyvesteyn, J. D. Fast, and J. J. de Jong, Report on some research in the field of magnetism at Philips laboratories, J. Phys. Radium **20**, 360 (1959).

[13] S. Mangin, D. Ravelosona, J. A. Katine, M. J. Carey, B. D. Terris, and Eric E. Fullerton, Current-induced magnetization reversal in nanopillars with perpendicular anisotropy, Nat. Mater. **5**, 210 (2006).

[14] Rie Matsumoto, Hiroko Arai, Shinji Yuasa, and Hiroshi Imamura, Spin-transfer-torque switching in a spin-valve nanopillar with a conically magnetized free layer, Appl. Phys. Express **8**, 063007 (2015).

[15] Hiroaki Yoda *et al.*, High efficient spin transfer torque writing on perpendicular magnetic tunnel junctions for high density MRAMs, Curr. Appl. Phys. **10**, e87 (2010).

[16] W. S. Zhao, Y. Zhang, T. Devolder, J. O. Klein, D. Ravelosona, C. Chappert, and P. Mazoyer, Failure and reliability analysis of STT-MRAM, Microelectron. Reliab. **52**, 1848 (2012).

[17] Y. Zhang, W. Wen, and Y. Chen, The prospect of STT-RAM scaling from readability perspective, IEEE Trans. Magn. **48**, 3035 (2012).

[18] William Fuller Brown, Thermal fluctuations of a single-domain particle, Phys. Rev. **130**, 1677 (1963).

[19] J. M. Shaw, H. T. Nembach, M. Weiler, T. J. Silva, M. Schoen, J. Z. Sun, and D. C. Worledge, Perpendicular magnetic anisotropy and easy cone state in $Ta/Co_{60}Fe_{20}B_{20}/MgO$, IEEE Magn. Lett. **6**, 1 (2015).

[20] Yu Fu, I. Barsukov, Jing Li, A. M. Gonçalves, C. C. Kuo, M. Farle, and I. N. Krivorotov, Temperature dependence of perpendicular magnetic anisotropy in CoFeB thin films, Appl. Phys. Lett. **108**, 142403 (2016).

[21] A. A. Timopheev, R. Sousa, M. Chshiev, H. T. Nguyen, and B. Dieny, Second order anisotropy contribution in perpendicular magnetic tunnel junctions, Sci. Rep. **6**, 26877 (2016).

[22] J. Z. Sun, Consequences of an interface-concentrated perpendicular magnetic anisotropy in ultrathin CoFeB films used in magnetic tunnel junctions, Phys. Rev. B **91**, 174429 (2015).

[23] D. Apalkov and W. H. Butler, U.S. Patent No. 8,780,665 (15 July 2014).

[24] Rie Matsumoto, Hiroko Arai, Shinji Yuasa, and Hiroshi Imamura, Theoretical analysis of thermally activated spin-transfer-torque switching in a conically magnetized nanomagnet, Phys. Rev. B **92**, 140409 (2015).

[25] H. Sato, E. C. I. Enobio, M. Yamanouchi, S. Ikeda, S. Fukami, S. Kanai, F. Matsukura, and H. Ohno, Properties of magnetic tunnel junctions with a MgO/CoFeB/Ta/ CoFeB/MgO recording structure down to junction diameter of 11 nm, Appl. Phys. Lett. **105**, 062403 (2014).

[26] G. Bertotti, I. D. Mayergoyz, and C. Serpico, *Nonlinear Magnetization Dynamics in Nanosystems*, Elsevier Series in Electromagnetism (Elsevier, New York, 2009).

[27] Yoshishige Suzuki, Ashwin A. Tulapurkar, and Claude Chappert, in *Nanomagnetism and Spintronics*, edited by Teruya Shinjo (Elsevier, Amsterdam, 2009), Chap. 3, pp. 93–153.

[28] M. D. Stiles and A. Zangwill, Anatomy of spin-transfer torque, Phys. Rev. B **66**, 014407 (2002).

[29] M. A. Zimmler, B. Özyilmaz, W. Chen, A. D. Kent, J. Z. Sun, M. J. Rooks, and R. H. Koch, Current-induced effective magnetic fields in Co/Cu/Co nanopillars, Phys. Rev. B **70**, 184438 (2004).

[30] Hitoshi Kubota, Akio Fukushima, Kay Yakushiji, Taro Nagahama, Shinji Yuasa, Koji Ando, Hiroki Maehara, Yoshinori Nagamine, Koji Tsunekawa, David D. Djayaprawira, Naoki Watanabe, and Yoshishige Suzuki, Quantitative measurement of voltage dependence of spin-transfer torque in MgO-based magnetic tunnel junctions, Nat. Phys. **4**, 37 (2008).

[31] Jack C. Sankey, Yong-Tao Cui, Jonathan Z. Sun, John C. Slonczewski, Robert A. Buhrman, and Daniel C. Ralph, Measurement of the spin-transfer-torque vector in magnetic tunnel junctions, Nat. Phys. **4**, 67 (2008).